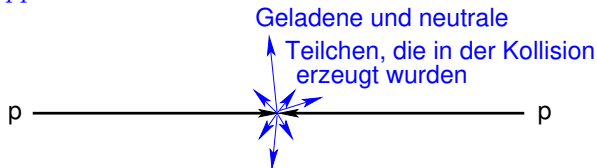


# Concepts of Experiments at Future Colliders II

PD Dr. Oliver Kortner

04.07.2025

## Topology of a $pp$ collision event



## Particles producible in the final state of a collision

### Leptons

- Neutrinos: stable, only weakly charged.  $\Rightarrow$  No interaction leading to a measurable electrical signal in the detector components.
- Electrons: stable, electrically charged.  $\Rightarrow$  Electrical signals in the detector components.
- Muons: unstable, but due to being ultrarelativistic, they are long-lived in the laboratory frame and do not decay in the detector; electrically charged.  $\Rightarrow$  Electrical signals in the detector components.
- $\tau$  leptons: unstable.  $\Rightarrow$  Detectable only through their decay products.

## Topology of a $pp$ collision event

### Additional particles producible in the final state of a collision

#### Hadrons

- In the elementary collision, quarks and gluons are initially produced. Due to confinement, these are not seen directly, but rather as so-called jets of hadrons, which originate from the quarks and gluons.
- Special role of two quarks:
  - b-quarks form long-lived b-hadrons, which allows the identification of b-quark jets.
  - t-quarks are so short-lived that they cannot form hadrons. They are detectable through their decay  $t \rightarrow Wb$ .

#### Photons

Photons are stable. Although they are electrically neutral, they can produce electromagnetic showers in matter, which can be detected by the detector.

# Recapitulation of the previous lecture

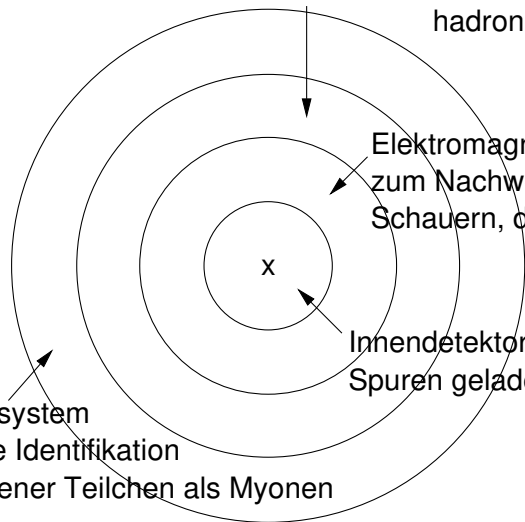
## Basic structure of a particle detector at a hadron collider

Hadronkalorimeter zum Nachweis  
hadronischer Schauer

Elektromagnetisches Kalorimeter  
zum Nachweis von elektromagnetischen  
Schauern, die von  $e^{\pm}$  und  $\gamma$  stammen

Innendetektor zur Messung der  
Spuren geladener Teilchen

Myonsystem  
für die Identifikation  
geladener Teilchen als Myonen



## Reconstruction of muon tracks in the inner detector

Reconstruction of muon trajectories is in a certain sense the simplest, because the energy loss of muons in the inner detector is negligible, and the trajectory therefore depends only on the following parameters:

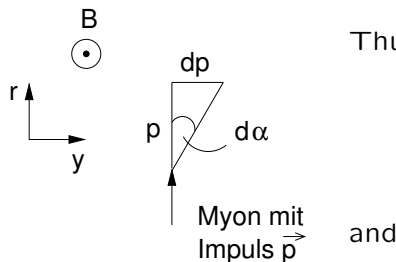
- $\vec{x}_0, \vec{p}$  at the interaction point.
- Magnetic field in the inner detector.
- Multiple scattering in the inner detector.

The reconstruction of muon tracks, as well as particle tracks in general, occurs in two interconnected steps: the so-called **pattern recognition**, where the hit points in the inner detector corresponding to the particle track are found, and the so-called **track fitting**, where the trajectory is calculated from the hit points selected during pattern recognition.

# Recapitulation of the previous lecture

## Trajectory in a magnetic field

$$d\alpha = \frac{dp}{p} = \frac{qvBdt}{p} = \frac{q}{p} B \underbrace{vdt}_{=ds=dr} = \frac{q}{p} B ds.$$



Thus, we obtain

$$\alpha(r) \approx \frac{q}{p} \int_{r_0}^r B(s) ds$$

and

$$y(r) = \int_{r_0}^r \alpha(r') dr' = \frac{q}{p} \int_{r_0}^r \int_{r_0}^{r'} B(s) ds dr'.$$

**Example.**  $p = 1 \text{ GeV}$ .  $r_0 = 0$ .  $B = 2 \text{ T}$ .

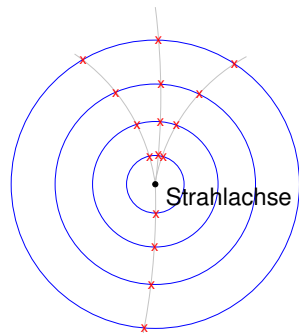
$\alpha(10 \text{ cm}) = 60 \text{ mrad}$ .  $y(10 \text{ cm}) = 3 \text{ mm}$ .

$\alpha(1 \text{ m}) = 0.6 \text{ rad}$ .  $y(1 \text{ m}) = 30 \text{ cm}$ .

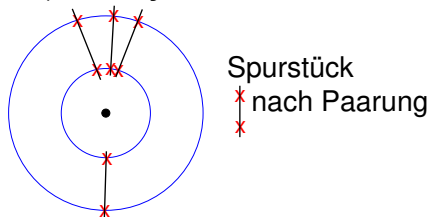
# Recapitulation of the previous lecture

## A possible method for pattern recognition

1. Consider all pairs of hits near the beamline sequentially.

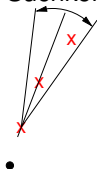


- Tatsächliche Flugbahn
- Detektorebene
- x Trefferpunkt



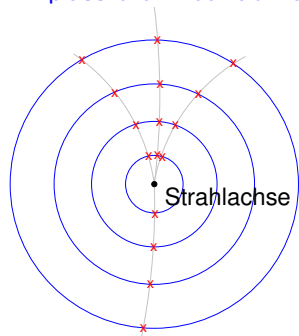
2. Search for hits in search corridors around the extrapolated track segments outward.

Suchkorridor



The size of the search corridor determines the smallest measurable momentum  $p$ .

## A possible method for pattern recognition

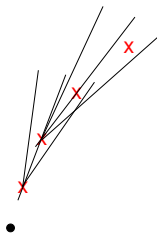


— Tatsächliche Flugbahn

— Detektorebene

x Trefferpunkt

3. Continue the extrapolation to the outermost measurement layer of the inner detector.



Two possibilities:

- (a) Size of the search corridor constant.
- (b) Size of the search corridor depends on the trajectory of the hits found so far.

# Recapitulation of the previous lecture

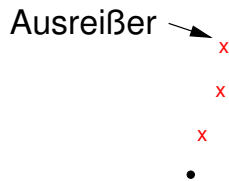
## Track fitting

Now consider all clusters of hits found during pattern recognition one by one.

Ideal case: Only one hit in each detector layer, no outliers.



Situation with so-called outliers



Situation with more than one hit in a layer



## Track fitting in the ideal case

x

- Hit coordinates:  $\vec{x}_1, \dots, \vec{x}_n$ .

x

- Position uncertainties:  $\sigma_1, \dots, \sigma_n$ .

x

- Uncertainties in detector positions, known as alignment uncertainties, lead to non-zero off-diagonal elements in the covariance matrix  $Cov(x_k, x_\ell)$ .

x

- Incorporate the influence of multiple scattering by introducing scattering centers, where the trajectory can bend.

- Track function:  $\vec{y}_k = \vec{y}_k(\frac{q}{p}, \vec{x}_0, \hat{p})$ .

- Determination of  $\frac{q}{p}$ ,  $\vec{x}_0$ , and  $\hat{p}$  using the method of least squares:

$$Q^2 = \sum_{k,\ell=1}^n (\vec{x}_k - \vec{y}_k)^t Cov(\vec{x}_k, \vec{x}_\ell) (\vec{x}_\ell - \vec{y}_\ell).$$

## Handling outliers and ambiguities

### Handling outliers

**Option 1.** Iterative approach: Track fitting including outliers. Then identify outliers from this track. Repeat track fitting excluding these identified outliers.

**Option 2.**  $\sigma_k = \bar{\sigma}_k$  for  $|\vec{x}_k - \vec{y}_k| < \delta$ ,  $\sigma_k \rightarrow \infty$  for  $|\vec{x}_k - \vec{y}_k| \geq \delta$ . This makes the contribution of outliers to  $Q^2$  negligibly small.

### Handling ambiguities

$\sigma_k = \sigma(|\vec{x}_k - \vec{y}_k|)$  as above, including all hits.

Alternatively, perform track fitting with all possible hit combinations and select the track with the smallest  $Q^2$ .

## Reconstruction of pion tracks in the inner detector

- $m_{\pi^\pm} \approx m_{\mu^\pm} \Rightarrow$  Pion tracks are very similar to muon tracks.
- $\pi \rightarrow \mu\nu_\mu$  decays are very rare in the lab frame due to time dilation. However, because so many  $\pi^\pm$  are produced in  $pp$  collisions, it happens with non-negligible frequency that a charged pion decays within the inner detector. At the decay point, the track bends.
- The size of this bend must be taken into account, at least in the size of the hit search corridors.

## Reconstruction of electron tracks in the inner detector

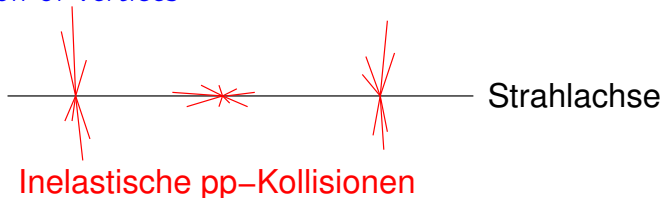
$m_{e^\pm} \ll m_{\pi/\mu}$ .  $\Rightarrow$  Energy loss in the inner detector is not negligible!

Two effects must be considered:

- Continuous energy loss due to synchrotron radiation.
- Discrete, large energy loss due to bremsstrahlung after scattering on atomic nuclei of the detector material.

**Common Procedure.** If tracks reconstructed with the standard algorithm for pions can be associated with a cluster of energy depositions in the electromagnetic calorimeter, these tracks are reconstructed again under the assumption that they are electron tracks. This process takes into account the hit search and the track model for continuous and discrete energy loss.

## Determination of vertices

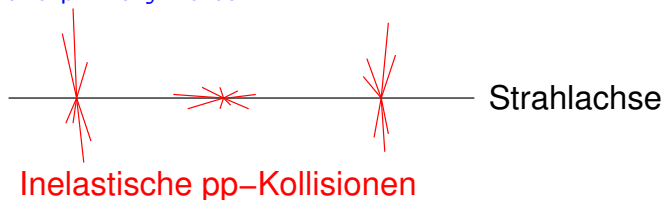


Position of a  $pp$  Collision: Primary vertex candidate.

## Determination of a Primary Vertex Candidate

- Collection of reconstructed particle tracks that cluster along the beam axis at a specific point.
- Determination of the precise vertex position using the method of least squares for the tracks' distance from the vertex.

## Selection of the primary vertex



## Selection of the primary vertex

In inelastic  $pp$  collisions, tracks are typically produced at small angles with respect to the beam axis. Therefore, in these collisions, the sum  $\Sigma$  of the transverse momentum magnitudes of the reconstructed particle tracks is small. This contrasts with collisions where a heavy particle is produced, where the transverse momenta of the decay products of this particle are large. Therefore, the primary vertex is usually selected as the primary vertex candidate with the maximum  $\Sigma$ .

## Simply described

$e^\pm$  = Inner detector tracks that can be associated with a cluster of energy deposits in the electromagnetic calorimeter.

## Properties of the cluster of energy deposits

- Lateral extension consistent with the Moli radius.
- Longitudinal extension confined to the electromagnetic calorimeter and corresponding to the length of an electromagnetic shower for the deposited energy in the calorimeter.

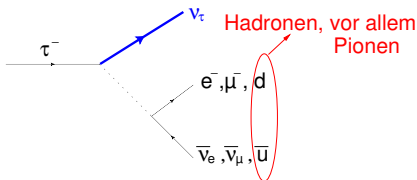
## Momentum determination

- $\hat{p}$ , flight direction of the electron or positron, equal to the direction of the electron track at the primary vertex.
- $E$ , electron energy, equal to the energy of the shower measured in the calorimeter. Reason: Energy measurement ( $\propto \frac{1}{\sqrt{E}}$ ) is more accurate than momentum measurement in the inner detector ( $\propto E$ ).

$\mu^\pm$  = Inner detector track that extends into the muon system.

**Requirement.** Energy deposited in the calorimeters near the muon is small, as muons lose very little energy in matter.

# Identification of $\tau$ leptons



- $\nu_\tau$  invisible.  $\Rightarrow E_\tau$  not measurable!

- Leptonic decay:

$$\tau^- \rightarrow e^- + \bar{\nu}_e + \nu_\tau \quad (18\%),$$

$$\tau^- \rightarrow \mu^- + \bar{\nu}_\mu + \nu_\tau \quad (17\%).$$

$\nu_\tau, \bar{\nu}_{e/\mu}$  invisible.

$e^-, \mu^-$  visible.

Decay recognizable through event topology.

- So-called hadronic  $\tau$  decays:

$$\tau^- \rightarrow \pi^- + \pi^0 + \nu_\tau \quad (25\%),$$

$$\tau^- \rightarrow \pi^- + 2\pi^0 + \nu_\tau \quad (9\%).$$

1 pion track, highly collimated jet from calorimeter clusters.

$$\tau^- \rightarrow 2\pi^- + \pi^+ + \nu_\tau \quad (9\%),$$

$$\tau^- \rightarrow 2\pi^- + \pi^+ + \pi^0 + \nu_\tau \quad (5\%).$$

3 pion tracks (one with opposite charge to the others), highly collimated jet from calorimeter clusters.

# Missing transverse momentum

- At the high center-of-mass energies we consider, the partons of the colliding protons interact with each other.
- Let  $\parallel$  denote the momentum component parallel to the proton beam axis, and  $\perp$  the momentum component perpendicular to it. Then, for the sum of the two parton momenta, we have

$$\begin{aligned}p_{1,\parallel} + p_{2,\parallel} &= x_1 \cdot p_{Proton} - x_2 \cdot p_{Proton} = (x_1 - x_2) \cdot \sqrt{s} \\p_{1,\perp} + p_{2,\perp} &= 0.\end{aligned}$$

This means that the longitudinal momentum sum fluctuates from  $pp$  collision to  $pp$  collision, but the transverse momentum sum always vanishes.

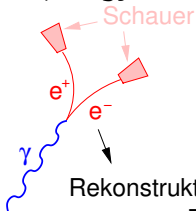
- From this, it follows that the sum of the transverse momenta of all particles in the final state of a  $pp$  collision also vanishes.
- If neutrinos (or other weakly interacting particles) appear in the final state, this can manifest as a non-zero sum of transverse momenta. This is referred to as **missing transverse momentum** or **missing transverse energy**.

# Identification of photons

Ideally  $\gamma$  = Cluster of energy deposits in the electromagnetic calorimeter that cannot be associated with an inner detector track.

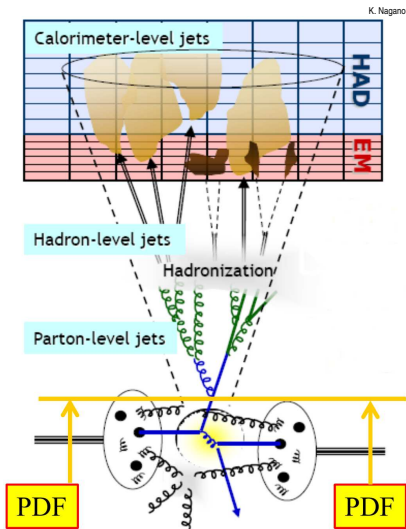
- Properties of the cluster similar to those of electrons and positrons.
- Main background  $\pi \rightarrow \gamma\gamma$  can be suppressed by requiring that the photon candidate does not lie within a jet.
- Non-negligible with inner detectors using semiconductor detectors: conversion  $\gamma \rightarrow e^+e^-$ .

Topology:



Rekonstruktion dieser Spuren nur möglich, wenn man Treffer von außen nach innen im Innendetektor sucht.

$e^+$  and  $e^-$  tracks must have a common vertex and be identified as electrons and positrons.



Quarks and gluons that are originally produced are not directly visible. Instead, the bundles of hadrons that arise from the original quarks and gluons, the so-called **jets**, are visible.

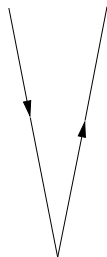
## Jet reconstruction at different levels

- Theory (at generator level): **parton jets**.
- Simulation: Jets from the generated hadrons, so-called **particle jets**.
- Detector, experiment: Jets from the signals produced by the hadrons; e.g., energy deposits in the calorimeters or the measured particle tracks.

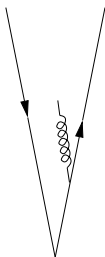
**Goal:** Matching detector jets to parton jets.  
Matching parton jets to the original quarks and gluons.

# Requirements for jet reconstruction

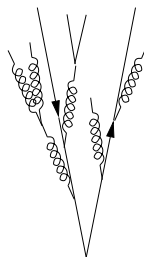
Goal: Stability.



Partonen in führender  
Ordnung Störungstheorie (LO)



Partonen in NLO

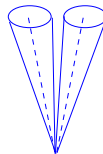
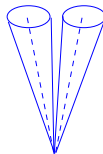
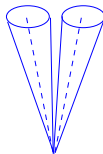
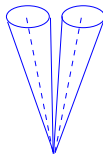


Partonenschauer

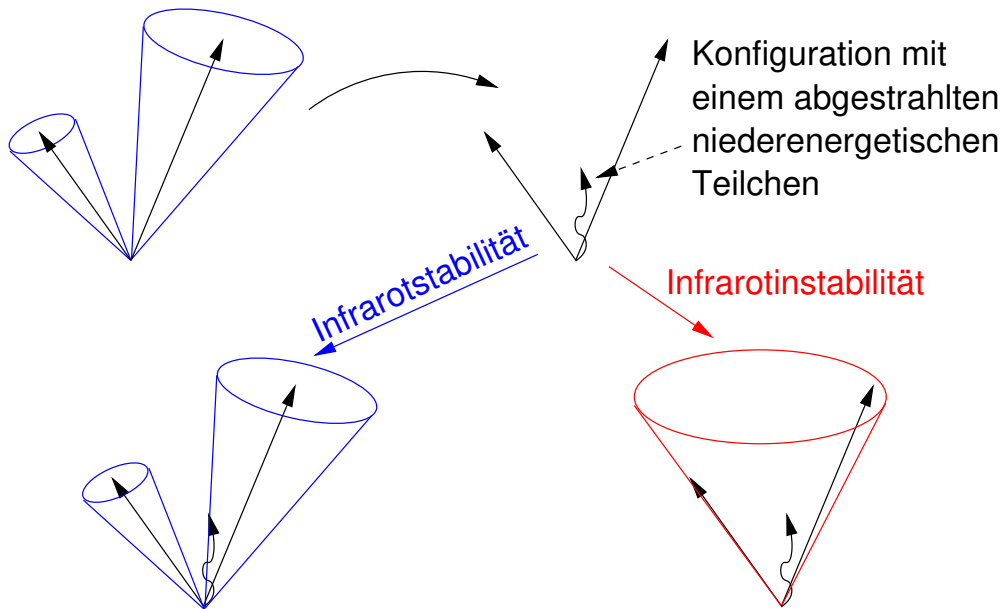


Hadronen

## Jets

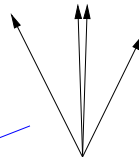
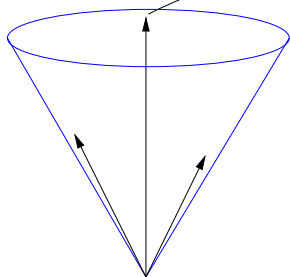


The definition of a jet is inherently ambiguous and depends on the jet algorithm used. It is crucial that the jet definition remains unchanged under certain changes in topology.

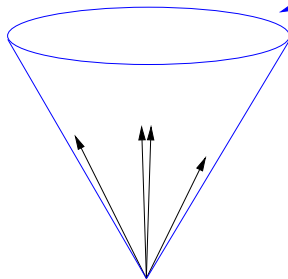


# Collinearity stability

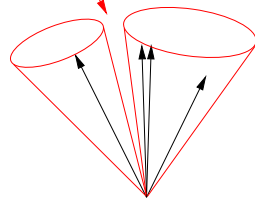
Ersetzen eines Teilchens durch  
zwei kollineare Teilchen



Kollinearitätsstabilität



Kollinearitätsinstabilität



**Goal:** Insensitivity to detector properties.

**Specifically**

- Independence of jet reconstruction efficiency from detector technology.
- Minimal impact of detector spatial and energy resolution on jet kinematics.
- Low sensitivity to detector noise, especially on the jet energy scale. Jet energy should not shift when the detector noise level changes.
- Low sensitivity to the number of inelastic collisions within an event.
- Low sensitivity to contributions from the proton remnants in a hard parton collision. This is often referred to as underlying event contribution.

**Other important properties:** Easy calibration of jet energy measurement; high jet reconstruction efficiency; ability to resolve nearby jets.

- Definition of a measure  $d_{ab}$  for the distance between two particles “ $a$  and  $b$ .”
- Combination algorithm
  - Calculate  $d_{ab}$  for all pairs of particles to determine the minimum distance  $d_{min}$ .
  - If  $d_{min}$  falls below a chosen threshold  $d_S$ , combine  $a$  and  $b$  into a single particle.
  - If  $d_{min} > d_S$ , consider  $a$  as a jet and remove it from the list of particles to be paired.
  - Repeat the process until  $d_{ab} > d_S$  for all pairs  $(a, b)$ .

The distance measure determines the geometric shape of the jet.

# The anti- $k_T$ algorithm

Algorithm used at the LHC: [Anti- \$k\_T\$  algorithm](#).

$p_{T,a}$ : Transverse momentum of particle  $a$ .

$d_{ab}$

$$d_{ab} := \min \left( \frac{1}{p_{T,a}}, \frac{1}{p_{T,b}} \right) \cdot \frac{\Delta_{ab}^2}{R^2}. \quad \Delta_{ab}^2 := (y_a - y_b)^2 + (\phi_a - \phi_b)^2.$$

$R$ : chosen radius parameter.  $y$ : rapidity.  $\phi$ : azimuthal angle.

$d_{a,B} := \frac{1}{p_{T,a}}$ : Measure of distance from the proton beam, used as  $d_S$ .

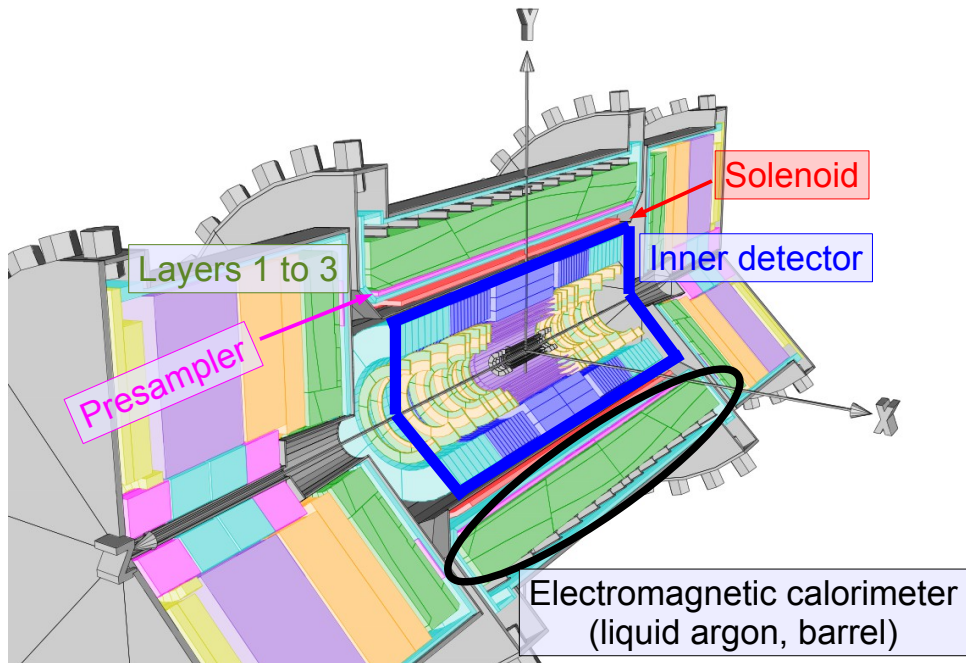
## Properties

- Initially pairs high-energy particles, then pairs high-energy particles with low-energy particles. Pairs of two low-energy particles are suppressed.
- Jets contain at least one high-energy particle.
- Jets resemble cone-like structures.
- Algorithm ensures infrared and collinearity stability, insensitivity to underlying event and number of inelastic  $pp$  collisions in an event.

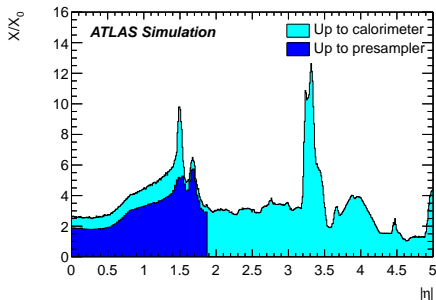
- Jets originating from  $b$ -quarks contain at least one  $b$ -hadron.
- $b$ -hadrons are long-lived. They decay at a certain distance from the primary vertex within the jet.
- By reconstructing this decay vertex, known as the secondary vertex,  $b$ -jets can be identified.

- The behavior of various reconstruction and identification techniques (track reconstruction, calorimeter cluster reconstruction, electron identification, jet reconstruction, etc.) must be validated using experimental methods.
- Examples of such quantities include:
  - Reconstruction or identification efficiency.
  - Misreconstruction or misidentification probability.
  - Energy or momentum scale.
  - Energy or momentum resolution.
- Here we will look at the calibration of the  $e/\gamma$  energy scale as an example.

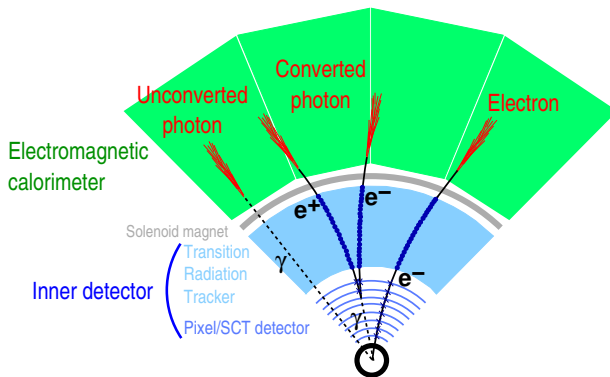
# ID and electromagnetic calorimeter for $e/\gamma$ detection



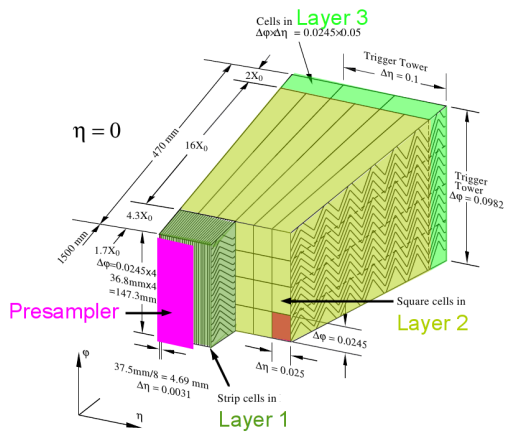
# Electron and photon reconstruction



- Significant material before the electromagnetic calorimeter ( $\sim 2X_0$ ).
- ⇒ Non-negligible probability of  $\gamma \rightarrow e^+e^-$  conversions before the calorimeter.
- ⇒ **3 topologies to consider:**



# Calibration of the $e/\gamma$ energy scale

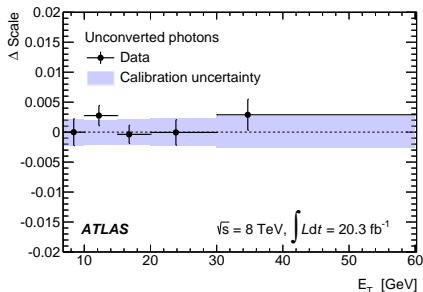
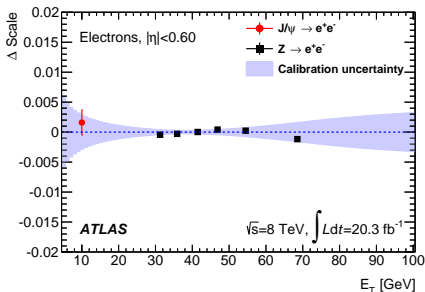


1. Cell energy calibration with test pulses.
2. Alignment of different calorimeter layers
  - No muon energy loss before the ECAL.
  - ⇒ Alignment of layers 1 to 3 using muons from  $Z$  decays.
  - Relative calibration of the presampler with electrons depending on the longitudinal shower development in the ECAL.
3. Determination of material in front of the electromagnetic calorimeter
  - Measurement of material between the presampler and the first layer with unconverted  $\gamma$ s depending on the longitudinal shower development.
  - Total material in front of the presampler is extracted from the difference in longitudinal shower profiles of electrons and unconverted photons.
4. Global calorimeter energy adjustment with  $Z \rightarrow e^+e^-$  decays.

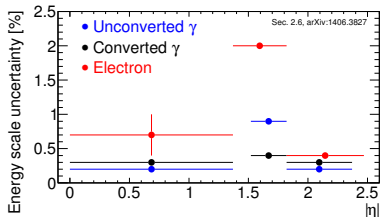
# Determination of energy scale uncertainty

## Verification of the $e/\gamma$ energy scale

- $J/\psi \rightarrow e^+e^-$  sensitive to the  $e^\pm$  energy scale for  $E_T \sim 7 \dots 35$  GeV.
- $Z \rightarrow \ell^+\ell^-\gamma$  sensitive to the photon energy scale for  $E_T \sim 30$  GeV.



## Total energy scale uncertainty



## Main sources of uncertainties

- Non-linearity of energy measurement at cell level:  $\sim 0.1\%$ .
- Alignment of calorimeter layers:  $\sim 0.1\%$ .
- Material in front of the calorimeter:  $0.1 \dots 0.3\%$ .